Tailored Amphiphilic Molecular Passivator for Stable Perovskite Solar Cells with 23.5 % Efficiency

Hongwei Zhu[1,2,3*], Yuhang Liu[2*†], Felix T. Eickemeyer[2*], Linfeng Pan[4], Dan Ren[2], Marco Ruiz[2], Brian Carlsen[4], Bowen Yang[4], Shirong Wang[1,3], Zaiwei Wang[4], Hongli Liu[1,3], Shaik M. Zakeeruddin[2], Anders Hagfeldt[4], M. Ibrahim Dar[2], Xianggao Li[1,3†], Michael Grätzel[2†].

1. *Tianjin University, School of Chemical Engineering and Technology, Tianjin 300072, China*
2. *Laboratory of Photonics and Interfaces (LPI), Department of Chemistry and Chemical Engineering, École Polytechnique Fédérale de Lausanne, Lausanne CH-1015, Switzerland.*
3. *Collaborative Innovation Center of Chemical Science and Engineering, Tianjin 300072, China*
4. *Laboratory of Photomolecular Science (LSPM), École Polytechnique Fédérale de Lausanne, Station 6, CH-1015 Lausanne, Switzerland.*

[†]Correspondance to: Dr. Yuhang Liu, yuhang.liu@epfl.ch, Prof. Xianggao Li, lixianggao@tju.edu.cn, Prof. Michael Graetzel, michael.graetzel@epfl.ch.

[*]These authors contributed equally.

Abstract

Passivation of interfacial defects serves as an effective means to realize highly efficient and stable perovskite solar cells (PSCs). However, most molecular modulators currently used to mitigate such defects form poorly conductive aggregates at the perovskite interface with the charge collection layer, impeding the extraction of photogenerated charge carriers. Here, we introduce the judiciously engineered passivator 4-tertbutylbenzylammonium iodide (tBBAI), whose bulky *tert*-butyl groups prevent the unwanted aggregation by steric repulsion. We find that the simple surface treatment with tBBAI accelerates significantly the charge extraction from the perovskite into the spiro-MeOTAD hole transporter, while retarding the non-radiative charge carrier recombination. This boosts the power conversion efficiency (PCE) of the PSC from 20% to 23.5% reducing the hysteresis to barely detectable levels. Importantly, the tBBAI treatment raises the fill factor from 0.75 to the very high value of 0.82, which concurs with a decrease in the ideality factor from 1.72 to 1.34, confirming the suppression of radiation-less carrier recombination. The *tert*-butyl group also provides a hydrophobic umbrella protecting the perovskite film from attack by ambient moisture. As a result, the PSCs show excellent operational stability retaining over 95% of their initial power conversion efficiency after 500 h full sun illumination under maximum power point (MPP) tracking under continuous simulated solar irradiation.

Introduction

Perovskite solar cells (PSCs) have attracted intense research interest due to their outstanding photovoltaic performance and low-cost together with large-area fabrication ability[1-3]. The power conversion efficiency (PCE) for PSCs increased dramatically from ~9% to 25.2% within the past few years[4, 5], with a concomitant increase in stability[6-9]. A typical PSC consists of an organic lead trihalide perovskite film that is sandwiched in between a hole-transporting layer (HTL) and an electron-transporting layer (ETL) for selective charge carrier extraction. Currently, the most successful ETL materials are tin dioxide (SnO_2) and titanium dioxide (TiO_2), referring to planar and mesoscopic structured PSCs. Both ETL materials exhibit outstanding electron selectivity and conductivity[10, 11], enabling high performing PSCs with efficiency up to 23.3%[12] and 23.7%[1]

respectively. The state-of-the-art HTL materials are organic materials bearing triphenylamine moieties (such as spiro-OMeTAD and PTAA) to ensure the hole-transport, while such organic materials are intrinsically hydrophobic and non-polarized, resulting in contact issues of the interface between the perovskite and HTL[13]. Moreover, due to the polycrystalline nature of solution processed perovskite layers, large amounts of defects, such as grain boundaries and vacancies form during fabrication process[14-18]. The photovoltage of PSCs depends on the dynamics of charge carrier recombination which occurs in the bulk or at the interface[19, 20]. Seo et al. report a double-layered halide architecture to overcome sluggish hole transfer from the perovskite to HTL, and achieved a PCE up to 22.7% [21]. Sherkar et al. showed that trap-assisted recombination at the interface between HTL and the perovskite is the dominant loss mechanism[22]. Thus, surface passivation of the perovskite is considered the most effective approach to suppress non-radiative recombination losses and, concomitantly, improve the photovoltage[23]. Mahdi et al showed that by surface passivation of the perovskite with adamantine amine a PCE of 20.93% can be achieved for mesoscopic PSCs[24]. A recent report by Jiang et al. indicates that highly efficient planar PSCs can achieve 23.3% with perovskite surface passivation with phenylethylammonium iodide (PEAI)[12].

In this work, we attain a PCE of 23.5 % by judicious tailoring of a defect mitigating agent based on benzylammonium iodide. We conceived and synthesized the new molecular passivator 4-*tert*-butyl-benzylammonium iodide (tBBAI). The latter exhibits an outstanding passivation ability as implied by increased photoluminescence quantum yield (PLQY) accompanied by larger quasi-Fermi level splitting (ΔE_F) in the perovskite films, resulting in a high open circuit voltage (V_{OC}) of 1.142 V. It is worth noting that the perovskite we use is iodide-rich with I:Br = 97:3, with an optical bandgap as low as 1.55 eV. Therefore, the voltage loss of the optimized device is ~410 mV, approaching 90% of the radiative limit. This is considered as one of the lowest voltage losses for PSCs. Time-resolve photoluminescence (TRPL) experiments reveal that the PSCs with a tBBAI interfacial layer show enhanced charge transfer from the perovskite layer to HTL than the control devices, presumably related to a reduced hole-extraction barrier due to a better contact between highly polarized perovskite layer and the non-polarized HTL, resulting in a significant improvement in fill factor (FF) of 82.1% than 78.5%. In addition, the device with more hydrophobic *tert*-butyl substitution endowed tBBAI passivated perovskite, the better resistivity to moisture. These results combined, highly efficient mesoscopic PSCs has been achieved with PCE up to 23.5%, where V_{OC} and FF are as high as 1.142 V and 82.1%, respectively. In addition to the outstanding photovoltaic (PV) performance, tBBAI passivated PSCs retained over 95% of their initial efficiency during photovoltaic operation for a period of 500 h under simulated full-sun irradiation.

Surface morphology of passivated perovskites

PEAI is one of the most widely used passivation agents reported so far[25-27]. While with enhanced photovoltaic performance and operational stability compared to non-passivated PSCs, incremental studies on chemical tailoring of PEAI are rare. Our previous study proved that by substituting the hydrogen (H) of the benzene ring with fluorine (F), the free energy of the perovskite surface was significantly reduced, endowing the perovskite with superior stability against moisture in ambient air[13]. The perovskite layer $Cs_{0.05}FA_{0.85}MA_{0.10}Pb(I_{0.97}Br_{0.03})_3$ with 5% excess of PbI_2

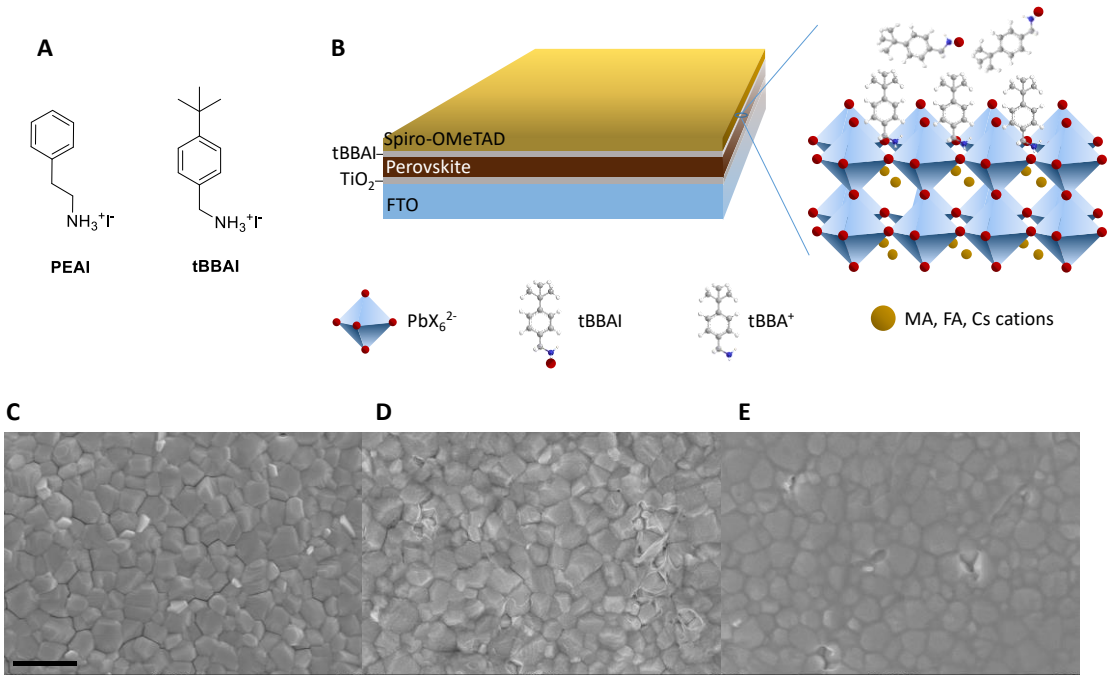

Figure 1A, chemical structures of PEAI and tBBAI. **B**, structures of a tBBAI passivated PSC, (**C, D, and E**) SEM images of a neat perovskite film, a perovskite film passivated by PEAI and a perovskite film passivated with tBBAI, respectively. The scale bar is 1 µm.

was fabricated using anti-solvent method[28] and annealed at 120 °C for 20 min before applying the modulators. The passivation agent, PEAI and tBBAI were applied by spincoating on the perovskite surface with 15 mM solution in isopropanol (IPA) without further annealing (**Figure 1B**). The surface morphology of the PEAI and tBBAI passivated perovskite films is characterized by scanning electron microscopy (SEM) and the results are shown in **Figure 1C, 1D** and **1E.** For the untreated neat perovskite film, it is observed that the domain size of the perovskite crystals is around 500 nm. After passivating with PEAI and tBBAI, their appearance remains unchanged, implying that the surface passivation does not alter the morphology of the perovskite active layer.

Structural and energetic properties of the passivation layer

X-Ray photoelectron spectroscopy (XPS) is used to characterize the surface elemental properties of the passivated perovskite, and the results are summarized in **Figure 2A**, **2B** and **2C**. The C 1s spectra of all perovskite film surfaces are compared in **Figure 2B**. In the neat perovskite film, a C=O peak at ~288 eV is observed, which is related to the oxygen and water exposure of the surface of the perovskite film[12]. This peak is significantly suppressed in the XPS spectra of the passivated perovskite film, proving that surface passivation with PEAI and tBBAI can effectively protect the perovskite form oxygen and moisture in ambient air[12] A further XPS depth profiling for tBBAI passivated perovskite was carried out to reveal the out-of-plane direction elemental distribution as shown in **Figure 2C**. Compared to the spectra of the neat perovskite film (**Figure S1),** the I 3d signal gradient of perovskite/tBBAI starts at deeper part in the film, suggesting the tBBAI layer thickness of < 5 nm.

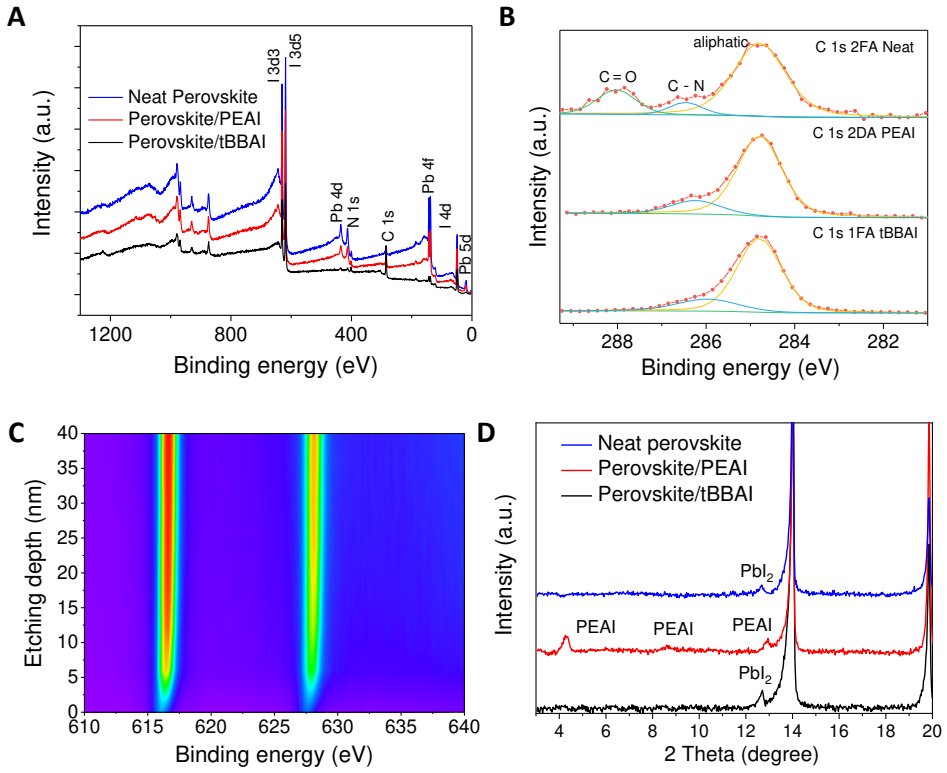

Figure 2. A, XPS survey spectra of neat perovskite, perovskite/PEAI and perovskite/tBBAI films. **B**, high-resolution deconvoluted carbon 1s spectra for various films. **C**, I 3d XPS depth profiles of the perovskite/tBBAI film. **D**, XRD patterns of neat perovskite, perovskite/PEAI and perovskite/tBBAI films

The structure of the unpassivated and passivated perovskite film is characterized by X-ray diffraction (XRD) As shown in **Figure S2.** The detailed XRD for $2\theta < 20°$ is shown in **Figure 2D**. Similar to a previous report[12], non-passivated perovskite film show excessive amount of PbI_2 at ~12.8°. For the PEAI passivated perovskite film, diffraction peaks corresponding to PEAI at 2θ = 4.3°, 8.6° and 12.9° are observed, implying crystalline PEAI on the surface of the perovskite film. The XRD spectrum of the tBBAI passivated perovskite film exhibits no extra diffraction peaks which suggests an amorphous morphology of the passivation layer. We attribute this result to an increased steric hindrance due to the *tert*-butyl substitution of tBBAI as compared to PEAI.

Optoelectronic quality

We investigated the optoelectronic quality of the perovskite film by time-resolved photoluminescence (TRPL) and steady-state absolute intensity photoluminescence (AIPL). TRPL measurements on samples with the structure glass/FTO/mp-Al_2O_3/perovskite/interface layer/ without and with HTL (Spiro-OMeTAD) are shown in **Figure 3**. For the samples without HTL (**Figure 3A**), at t > 200 ns after the excitation pulse the TRPL curves can be well fitted with a (mono-) exponential function with the decay times shown in **Table S1**. We observe a significant difference between the surface treatment with the two modulators: The decay time for the PEAI treated perovskite film is a factor of three and for tBBAI a factor of five higher than for the non-passivated film. We apply numerical simulations to model the TRPL measurements at times beyond 200 ns.

The details of these simulations are described in the supporting information (Note 1). Since the only difference between the samples are the surface layers, we fitted the numerical model to the data with only one free parameter, the surface recombination velocity *S*. For the sample with the longest decay time (tBBAI, black dots in **Figure 3b**) the decay could be caused not only by *S* but also by non-radiative bulk recombinations (with monomolecular recombination rate constant k_1, see **Supplementary Note**) or radiative bimolecular recombinations (with bimolecular recombination rate constant k_2). Therefore, three extreme cases are considered, where the PL decay at later times for tBBAI is caused exclusively by non-radiative (bulk) recombinations ($k_1 = k_1^{max}, k_2 = 0, S = 0$), by bimolecular radiative (bulk) recombinations ($k_2 = k_2^{max}, k_1 = 0, S = 0$), and by surface recombinations ($k_1 = k_2 = 0$). The *S*-fits for all these cases are summarized in supplementary **Table S1**. Taking into account these cases one can estimate the surface recombination velocity for the different samples, which is 33±3 cm/s for the control, 8±3 cm/s for PEAI and 3±3 cm/s for tBBAI which demonstrates the positive effect on surface defect passivation of PEAI and even more pronounced of tBBAI.

Figure 4A shows the external photoluminescence quantum yield ($PLQY_{ext}$) of the perovskite films with the different interface layers and with HTL measured at an excess carrier generation rate corresponding to 1 sun conditions. We determined the $PLQY_{ext}$ by AIPL measurements with the method described by de Mello et al[29], $PLQY_{ext} = \int P(E)\ dE / \int L_{in}(E)\ dE$, where P is the AIPL spectral photon flux and L_{in} is the spectral photon flux of the excitation beam. The respective AIPL data are shown in **Figure S3.**

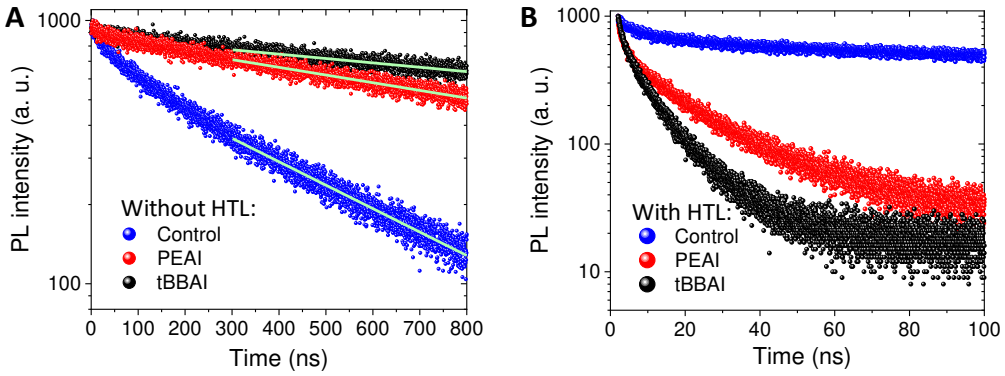

Figure 3. **A,** TRPL for the layer structure glass/FTO/compact-TiO_2/mesoscopic-TiO_2/perovskite/without surface layer (control, blue), with PEAI (red), and tBBAI (black). The fit curves using the model described in the main text are shown by green lines. **B**, TRPL measurements of HTL containing samples without interface layer, with PEAI, and with tBBAI.

The $PLQY_{ext}$ can be expressed in terms of the radiative (R_{rad}) and non-radiative (R_{nr}) recombination rates $PLQY_{ext} = R_{rad}/(R_{rad} + R_{nr})$ which makes it a useful tool to investigate bulk, interface, and surface charge recombination characteristics.

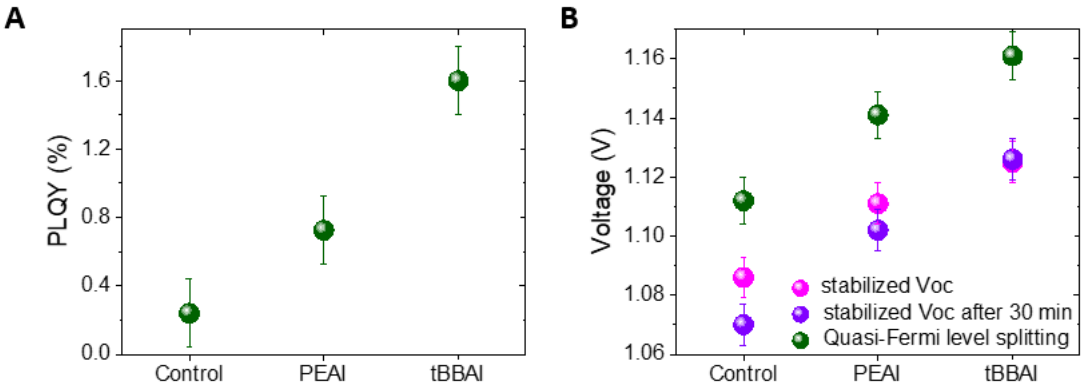

Figure 4: **A,** PLQY for the layer structure glass/FTO/c-TiO_2/mp-TiO_2/perovskite/interface layer/without and with HTL. **B**, Stabilized V_{OC} and Quasi-Fermi level splitting $\Delta E_F/q$ for the layer structure glass/FTO/compact-TiO_2/mesoscopic-TiO_2/perovskite/interface layer/HTL. The stabilized V_{OC} after 30 minutes' light soaking is also shown.

As shown in **Figure 4A,** the $PLQY_{ext}$ of PEAI is about 3-times and of tBBAI 8-times higher than the control sample without interface layer. The interface layers cause a significant decrease of interface recombinations at the perovskite/HTL interface which implies an improved defect chemistry. From $PLQY_{ext}$ the quasi-Fermi level splitting ΔE_F can be calculated with the following equation[30]:

$$\Delta E_F = q\ V_{OC,rad} + kT\ ln(PLQY_{ext}),$$

where $V_{OC,rad}$ is the radiative limit of V_{OC}, the calculation of which is shown in the supplementary information (Note 2). $\Delta E_F/q$ for the differently treated films is shown in **Figure 4B**. The PEAI treated film shows a ΔE_F increase of 28 meV and the tBBAI treated film an increase of 48 meV compared to the control sample without interface layer. Since $\Delta E_F/q$ is the maximum V_{OC} that a PSC with this layer structure can exhibit, we present measured V_{OC}'s of the complete PSCs with similar layer structure in **Figure 4B** as well. To be comparable with $\Delta E_F/q$, which is determined from quasi-steady state $PLQY_{ext}$ measurements, we measured the quasi-steady state V_{OC}'s, i.e. stabilized after two minutes exposure under 1 sun simulated illumination conditions. We also show the stabilized V_{OC}'s of the same samples after thirty minutes' light soaking under 1 sun in ambient air. With PEAI surface treatment the V_{OC} increased by 25 mV from 1.086 V to 1.111 V and with tBBAI by 41 mV to 1.125 V compared to the control sample, which is in good agreement with the trend seen in the ΔE_F measurements. The offset of ~40 mV between the stabilized V_{OC} and $\Delta E_F/q$ can be explained by energetic misalignment at both interfaces as has been shown by Caprioglio et al[31].

This demonstrates the beneficial effect of PEAI and tBBAI treatment in preventing interfacial charge carrier recombination. Furthermore, it shows that tBBAI is a significantly better interface passivation agent than PEAI with a 65% higher ΔV_{OC} increase compared to the sample without interface passivation layer. After 30 minutes under 1 sun light soaking the ΔV_{oc}'s are 32 mV for PEAI and 56 mV for tBBAI treated films which confirms the trend. Note that there is a 15 mV V_{OC} drop for the control sample, 9 mV drop for the PEAI, and a negligible V_{OC} drop for the tBBAI treated films. This shows that the interface layers used here also increase the short-term V_{OC} stability

under light soaking in ambient air and that tBBAI shows superior performance in comparison with PEAI.

To further demonstrate the effect of these interface layers on the optoelectronic properties, we measured the TRPL of the passivated perovskites films with HTL (**Figure 3B**). We attribute the rapid decay of the PL signal within the first 10 to 60 ns to three major processes: First, carrier diffusion leads to a fast decay of carrier concentration close to the front surface of the incident light pulse[32, 33]; Second, halide perovskites have a positively charged mid-gap trap state caused by iodide vacancies with a large capture cross-section for electrons. Once these trap states are filled they are neutral and, hence exhibit a very low capture cross-section for holes so that the hole lifetime is in the µs range[34, 35]. This fast electron capture leads to a rapid decay of the PL signal at early times. Third, hole injection into the HTL also causes a rapid decay of the PL signal with a rate proportional to the carrier concentration at the interface, which is highest within the first ~100 ns. Whereas the first two mechanisms are the same for all our samples, the third mechanism depends on the specific interface and HTL. Hence, the difference in TRPL for the first 60 ns is caused by different hole transfer rates into the HTL. The PEAI-treated film shows a significantly faster hole extraction into the HTL compared to the untreated film but it is outperformed by tBBAI. This faster charge transfer is very likely caused by a smaller hole transfer barrier and, concomitantly, by a lower hole transfer resistance. Due to the intrinsically high polarization of the perovskite material and the low polarization of the organic and hydrophobic Spiro-OMeTAD, we expect a hole transport barrier that is related to the poor contact of HTL and perovskite. With the ambipolar passivation agent bearing ammonium iodide that coordinates with the perovskite and hydrophobic ligand similar to that of HTL, the barrier shall be minimized. If we compare the difference between PEAI and tBBAI, less crystalline tBBAI is most probably creating more even coverage on the surface of the perovskite, creating better contact between HTL and perovskite.

Photovoltaic performance

To demonstrate the advantage of the new passivation agent in solar cells, PSCs are fabricated with tBBAI as passivation agent; for comparison, PEAI and non-passivated perovskites are applied. The PSCs have the n-*i*-p device architecture FTO/compact TiO_2/mesoscopic TiO_2/perovskite/PEAI or tBBAI/Spiro-OMeTAD/gold. IV curves of these cells under 1 sun illumination are shown in **Figure 5A** and the corresponding PV parameters in **Table 1**.

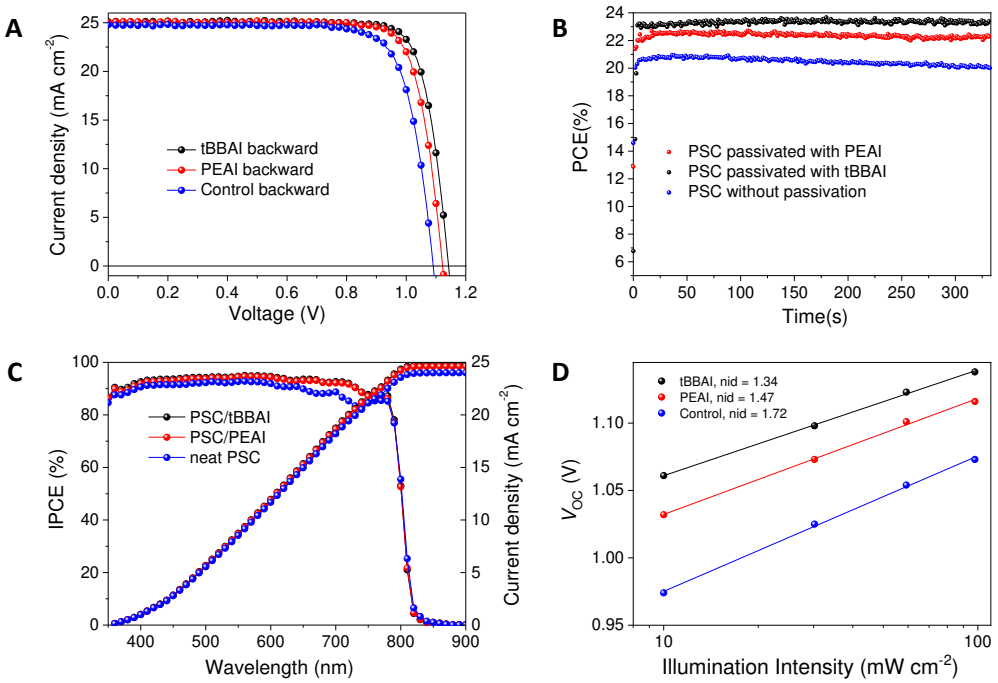

Figure 5. A, reverse *I-V* curves of the champion PSCs. **B,** MPP tracking of the PSCs within the first 330 s under ambient air. **C**, IPCE of the PSCs. **D**, V_{OC} dependence of light intensity with ideality factors n_{id}.

A champion cell with a PCE of 23.5% is achieved with tBBAI passivation, with a V_{OC} of 1142 mV, a fill factor (FF) of 82.1% and a J_{SC} of 25.1 mA cm^{-2}. This V_{OC} represents a voltage loss of 408 mV with respect to the optical bandgap of 1.550 eV (derived from the inflection point of the IPCE spectrum in **Figure 5C**), which is 89.9% of the radiative limit of V_{oc} of 1270 mV (see Note 2 in supplementary information). Negligible hysteresis of 1.8% and 0.8% is observed between the forward and reverse scan of PEAI and tBBAI, respectively. By contrast, the hysteresis of non-passivated PSC is as high as 5.5%, with 20.1% PCE for the forward scan and 21.2% for the reverse scan. The photovoltaic metrics in **Figure S5** depict the high reproducibility of the photovoltaic performance in this study. **Figure 5B** shows the stabilized power output at the maximum power point (MPP) for the best performing devices under dehumidified ambient air (10% RH) within the first 3 min. For tBBAI the stabilized PCE is 23.3%, which is in good agreement with the PCEs obtained from the forward and backward J-V scans. However, we observed a decrease with PSCs from initially 23.1% to 22.5% with PEAI as a passivator, which proves the superior performance of the tBBAI treated devices. Incident photon-to-current conversion efficiencies (IPCE) are shown in **Figure 5C**. The integrated photocurrent is in good agreement with the corresponding J_{SC} values measured from J-V curves (**Table 1**). **Figure 5D** shows the illumination intensity dependence of the V_{OC} from which the ideality factor n_{id} can be extracted. The unpassivated film has a n_{id} of 1.72, PEAI passivation leads to 1.47 and tBBAI passivation to 1.34. A n_{id} of 1 is expected for a film with only bimolecular radiative recombinations whereas a n_{id} of 2 indicates that all recombinations are non-radiative monomolecular[36]. tBBAI shows the n_{id} closest to 1 which indicates the lowest non-radiative recombination rate followed by PEAI and the unpassivated film which is in good agreement with the findings from the optoelectronic measurements.

Operational stability data obtained with PSCs at MPP under 1 sun irradiation and in nitrogen atmosphere (N_2) are shown in **Figure 6A**. After 500 hours, the PSC passivated by tBBAI interlayer retained 95% of its initial efficiency, in contrast to 84% for the PSC with PEAI interlayer and 70% for the non-passivated PSC. The major contribution to the efficiency decline observed for the latter PSCs arise stems from a decrease in FF (~87% compared to initial value), The reason for this is likely that the PEAI interlayer or the direct contact between perovskite and HTL does not form a stable interface as contrast to tBBAI. Contact angle measurements of water droplets on the surface of perovskite films with and without interfacial layers are shown in **Figure 6B**. The perovskite film with tBBAI surface treatment exhibits a contact angle up to 82^o, which is much higher compared to PEAI-treated and untreated perovskite films, implying a better moisture resistance[37]. To further prove this, PSCs with and without interface layers are aged under ambient condition with a RH (relative humidity) of 50-70 %, the results are shown in **Figure S6.** It is observed that after 55 days (~ 1300 h), the PSC with tBBAI interlayer decreased by less than 10%, while in comparison, PSC with PEAI decrease by 30% and PSCs without interface layer decreased by over 26%, This larger performance decrease implies a faster degradation of the perovskite films due to increased moisture uptake.

Table 1, photovoltaic parameters of champion devices with and without passivation agents (measured under simulated AM 1.5G irradiance)

PSC	V_{OC} [V]	J_{SC}[c] [mA cm^{-2}]	J_{SC}[d] [mA cm^{-2}]	FF	PCE [%]
Control-FWS[a]	1.077	24.87		0.750	20.1
Control-RVS[b]	1.091	24.79	24.01	0.785	21.2
tBBAI-FWS	1.142	25.11		0.815	23.4
tBBAI-RVS	1.142	25.10	24.90	0.821	23.5
PEAI-FWS	1.121	25.06		0.794	22.3
PEAI-RVS	1.122	25.01	24.95	0.809	22.7

[a]forward scan;

[b]reverse scan;

[c]J_{SC} determined from the IV measurement;

[d]J_{SC} determined from IPCE.

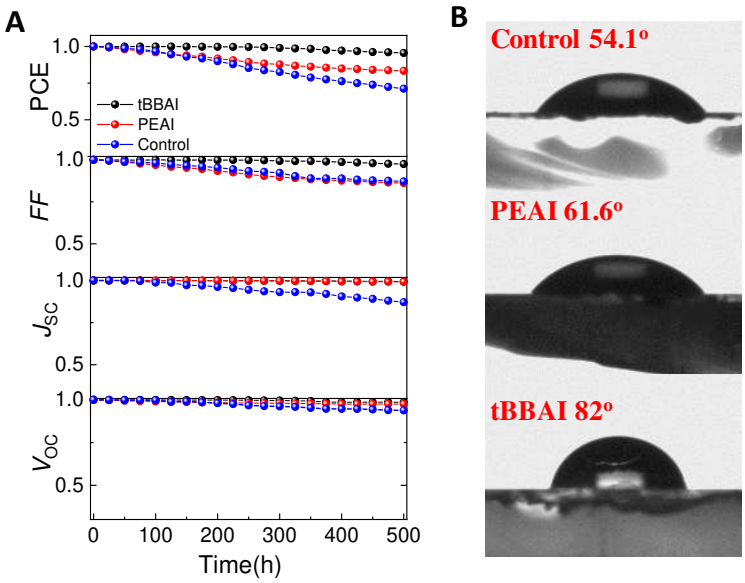

Figure 6. A, MPP ageing results in inert atmosphere (N_2) and under 1 sun continuous illumination of a PSC without passivation and PSCs passivated with PEAI and tBBAI. **B,** Images of water droplets on the surface of a neat perovskite film (control) and on passivated perovskite films.

Conclusion

In conclusion, a new surface passivation agent, tBBAI was developed. Electro-optical characterizations show that tBBAI passivated perovskite films exhibit less non-radiative charge carrier recombination, i.e. a lower defect density, and a significantly improved charge extraction from the perovskite film to the HTL. We observe a V_{OC} increase of ~ 20 mV with tBBAI compared to PEAI, and ~ 50mV compared to the perovskite films without passivation. Our tBBAI champion cell yielded PCE of 23.5%, which is among the highest PSC efficiencies achieved so far. In addition, the enhanced hydrophobicity of tBBAI compared to PEAI leads to an enhanced moisture resistivity, and thus better operational stability. PSCs with tBBAI retained over 95% of their initial PCE after 500 h MPP tracking, and over 90% of their initial PCE after 55 days ageing under ambient air with an RH of 50-70%. Our work provides a simple yet effective approach to fabricate efficient PSCs with outstanding efficiency and high operational stability.

Acknowledgement

H.Z. thanks the China Scholarship Council for funding. Y.L., S.M.Z., and M.G. thank the King Abdulaziz City for Science and Technology (KACST) and the European Union's Horizon 2020 research and innovation program (grant agreement No 826013) for financial support. X.L. acknowledges the financial support from the National Science Foundation of China (No. 21676188). B.Y. thank funding support from the European Union's Horizon 2020 research and innovation programme under grant agreement No 764047. D. R. thanks Sino-Swiss Science and Technology Cooperation (SSSTC) 2016 from Swiss National Science Foundation (IZLCZ2-170294).

[1] H. Min, M. Kim, S.-U. Lee, H. Kim, G. Kim, K. Choi, J. H. Lee, S. I. Seok, Science 2019, 366, 749.
[2] Y. Rong, Y. Hu, A. Mei, H. Han, A. Mei, H. Tan, M. I. Saidaminov, E. H. Sargent, H. Tan, S. I.

Seok, M. D. McGehee, Science 2018, 361.
[3] F. Ye, W. Tang, F. Xie, M. Yin, J. He, Y. Wang, H. Chen, Y. Qiang, X. Yang, L. Han, Adv. Mater. 2017, 29, 1701440.
[4] H.-S. Kim, C.-R. Lee, J.-H. Im, K.-B. Lee, T. Moehl, A. Marchioro, S.-J. Moon, R. Humphry-Baker, J.-H. Yum, J. E. Moser, M. Grätzel, N.-G. Park, Sci. Rep. 2012, 2, 591.
[5] NREL, National Renewable Energy Laboratory, 2019 https://www.nrel.gov/pv/cell-efficiency.html.
[6] S. Yang, S. Chen, E. Mosconi, Y. Fang, X. Xiao, C. Wang, Y. Zhou, Z. Yu, J. Zhao, Y. Gao, F. De Angelis, J. Huang, Science 2019, 365, 473.
[7] M. Saliba, T. Matsui, K. Domanski, J.-Y. Seo, A. Ummadisingu, S. M. Zakeeruddin, J.-P. Correa-Baena, W. R. Tress, A. Abate, A. Hagfeldt, M. Graetzel, Science 2016, 354, 206.
[8] D. Luo, W. Yang, Q. Hu, R. Su, Z. Xu, T. Liu, K. Chen, F. Ye, P. Wu, L. Zhao, J. Wu, Y. Tu, Y. Zhang, X. Yang, Q. Gong, R. Zhu, D. Luo, Q. Gong, R. Zhu, Z. Wang, H. J. Snaith, A. Sadhanala, R. Shivanna, R. H. Friend, G. F. Trindade, J. F. Watts, W. Zhang, Q. Gong, R. Zhu, Science 2018, 360, 1442.
[9] S. Bai, P. Da, C. Li, Z. Wang, Z. Yuan, F. Fu, M. Kawecki, X. Liu, N. Sakai, J. T.-W. Wang, S. Huettner, S. Buecheler, M. Fahlman, F. Gao, H. J. Snaith, Nature 2019, 571, 245.
[10] Q. Jiang, L. Zhang, H. Wang, X. Yang, J. Meng, H. Liu, Z. Yin, J. Wu, X. Zhang, J. You, Nat. Energy 2016, 2, 16177.
[11] W. S. Yang, J. H. Noh, N. J. Jeon, Y. C. Kim, S. Ryu, J. Seo, S. I. Seok, Science 2015, 348, 1234.
[12] Q. Jiang, Y. Zhao, X. Zhang, X. Yang, Y. Chen, Z. Chu, Q. Ye, X. Li, Z. Yin, J. You, Nat. Photonics 2019, 13, 460.
[13] Y. Liu, S. Akin, R. Uchida, N. Arora, J. V. Milic, A. R. Uhl, S. M. Zakeeruddin, M. I. Dar, M. Gratzel, S. Akin, L. Pan, A. Hagfeldt, R. Uchida, A. Hinderhofer, F. Schreiber, Sci. Adv. 2019, 5, eaaw2543.
[14] M. Abdi-Jalebi, Z. Andaji-Garmaroudi, A. J. Pearson, G. Divitini, S. Cacovich, B. Philippe, H. Rensmo, C. Ducati, R. H. Friend, S. D. Stranks, ACS Energy Lett. 2018, 3, 2671.
[15] F. Ji, S. Pang, L. Zhang, Y. Zong, G. Cui, N. P. Padture, Y. Zhou, ACS Energy Lett. 2017, 2, 2727.
[16] W. Li, Y.-Y. Sun, L. Li, Z. Zhou, J. Tang, O. V. Prezhdo, J. Am. Chem. Soc. 2018, 140, 15753.
[17] S. G. Motti, D. Meggiolaro, A. J. Barker, E. Mosconi, C. A. R. Perini, J. M. Ball, M. Gandini, M. Kim, F. De Angelis, A. Petrozza, Nat. Photonics 2019, 13, 532.
[18] F. Zhang, C. Xiao, X. Chen, B. W. Larson, S. P. Harvey, J. J. Berry, K. Zhu, Joule 2019, 3, 1452.
[19] M. Stolterfoht, C. M. Wolff, J. A. Marquez, S. Zhang, C. J. Hages, D. Rothhardt, S. Albrecht, P. L. Burn, P. Meredith, T. Unold, D. Neher, Nat. Energy 2018, 3, 847.
[20] W. Nie, H. Tsai, R. Asadpour, J.-C. Blancon, A. J. Neukirch, G. Gupta, J. J. Crochet, M. Chhowalla, S. Tretiak, M. A. Alam, H.-L. Wang, A. D. Mohite, Science 2015, 347, 522.
[21] E. H. Jung, N. J. Jeon, E. Y. Park, C. S. Moon, T. J. Shin, T.-Y. Yang, J. H. Noh, J. Seo, Nature 2019, 567, 511.
[22] T. S. Sherkar, L. J. A. Koster, C. Momblona, L. Gil-Escrig, J. Avila, M. Sessolo, H. J. Bolink, ACS Energy Lett. 2017, 2, 1214.
[23] J. J. Yoo, S. Wieghold, M. Sponseller, M. Chua, S. N. Bertram, N. T. P. Hartono, J. Tresback, E. Hansen, J.-P. Correa-Baena, V. Bulovic, T. Buonassisi, S. S. Shin, M. G. Bawendi, Energy Environ. Sci. 2019, 12, 2192.
[24] M. M. Tavakoli, D. Bi, L. Pan, A. Hagfeldt, S. M. Zakeeruddin, M. Graetzel, Adv. Energy Mater. 2018, 8, 1800275.

[25] K. Wang, Z. Jin, L. Liang, H. Bian, D. Bai, H. Wang, J. Zhang, Q. Wang, L. Shengzhong, Z. Jin, Q. Wang, L. Shengzhong, Nat. Commun 2018, 9, 4544.
[26] N. Li, Z. Zhu, C.-C. Chueh, H. Liu, B. Peng, A. Petrone, X. Li, L. Wang, A. K. Y. Jen, Adv. Energy Mater. 2017, 7, 1601307.
[27] M. Kim, G.-H. Kim, T. K. Lee, I. W. Choi, H. W. Choi, Y. Jo, Y. J. Yoon, J. W. Kim, J. Lee, D. Huh, H. Lee, S. K. Kwak, J. Y. Kim, D. S. Kim, Joule.
[28] N. Ahn, D. Y. Son, I. H. Jang, S. M. Kang, M. Choi, N. G. Park, J. Am. Chem. Soc. 2015, 137, 8696.
[29] J. C. de Mello, H. F. Wittmann, R. H. Friend, Adv. Mater. 1997, 9, 230.
[30] R. T. Ross, J. Chem. Phys. 1967, 46, 4590.
[31] P. Caprioglio, M. Stolterfoht, C. M. Wolff, T. Unold, B. Rech, S. Albrecht, D. Neher, Adv. Energy Mater. 2019, 5, 1901631.
[32] B. Wenger, P. K. Nayak, X. Wen, S. V. Kesava, N. K. Noel, H. J. Snaith, Nat. Commun 2017, 8, 590.
[33] A. A. B. Baloch, F. H. Alharbi, G. Grancini, M. I. Hossain, M. K. Nazeeruddin, N. Tabet, J. Phys. Chem. C 2018, 122, 26805.
[34] A. Walsh, D. O. Scanlon, S. Chen, X. G. Gong, S.-H. Wei, Angew. Chem., Int. Ed. 2015, 127, 1811.
[35] T. S. Sherkar, C. Momblona, L. Gil-Escrig, J. Ávila, M. Sessolo, H. J. Bolink, L. J. A. Koster, ACS Energy Letters 2017, 2, 1214.
[36] W. Tress, M. Yavari, K. Domanski, P. Yadav, B. Niesen, J. P. Correa Baena, A. Hagfeldt, M. Graetzel, Energy Environ. Sci. 2018, 11, 151.
[37] F. Zhang, W. Shi, J. Luo, N. Pellet, C. Yi, X. Li, X. Zhao, T. J. S. Dennis, X. Li, S. Wang, Y. Xiao, S. M. Zakeeruddin, D. Bi, M. Grätzel, Adv. Mater. 2017, 29, 1606806.